Applied Physics Letters ARTICLE pubs.aip.org/aip/apl

Electron mobility enhancement by electric field engineering of AlN/GaN/AlN quantum-well HEMTs on single-crystal AlN substrates

Cite as: Appl. Phys. Lett. **124**, 152111 (2024); doi: 10.1063/5.0190822
Submitted: 8 December 2023 · Accepted: 23 March 2024 ·
Published Online: 10 April 2024

View Online

Export Citation

CrossMark

Yu-Hsin Chen,[1,a] Jimy Encomendero,[2] Chandrashekhar Savant,[1] Vladimir Protasenko,[2] Huili (Grace) Xing,[1,2,3] and Debdeep Jena[1,2,3]

AFFILIATIONS

[1]Department of Materials Science and Engineering, Cornell University, Ithaca, New York 14853, USA
[2]School of Electrical and Computer Engineering, Cornell University, Ithaca, New York 14853, USA
[3]Kavli Institute at Cornell for Nanoscale Science, Cornell University, Ithaca, New York 14853, USA

[a]Author to whom correspondence should be addressed: yc794@cornell.edu

ABSTRACT

To enhance the electron mobility in quantum-well high-electron-mobility transistors (QW HEMTs), we investigate the transport properties in AlN/GaN/AlN heterostructures on Al-polar single-crystal AlN substrates. Theoretical modeling combined with experiment shows that interface roughness scattering due to high electric field in the quantum well limits mobility. Increasing the width of the quantum well to its relaxed form reduces the internal electric field and scattering, resulting in a binary QW HEMT with a high two-dimensional electron gas (2DEG) density of 3.68×10^{13} cm^{-2}, a mobility of 823 cm^2/Vs, and a record-low room temperature (RT) sheet resistance of 206 $\Omega/\square$. Further reduction of the quantum well electric field yields a 2DEG density of 2.53×10^{13} cm^{-2} and RT mobility > 1000 cm^2/V s. These findings will enable future developments in high-voltage and high-power microwave applications on the ultrawide bandgap AlN substrate platform.

Published under an exclusive license by AIP Publishing. https://doi.org/10.1063/5.0190822

10 April 2024 15:51:19

GaN-based high-electron-mobility transistors (HEMTs) are a leading platform in high-voltage and high-frequency applications due to their wide bandgap, high electron velocities, and the ability to form heterostructures, yielding high carrier concentration and high electron mobility.[1–5] GaN HEMTs primarily built with Al(Ga)N/GaN heterostructures on silicon, SiC, or sapphire substrates demonstrate high output power density,[6,7] which is now hitting the limitations posed by the thermal properties of GaN, and its interfaces and thermal properties of substrates that limit its operational lifetime and degrades their performance.[8–10] Several concerns on reliability of GaN HEMTs, such as trap effects and breakdown voltages, remain unresolved.[11]

To meet the demand for high-power and high-frequency operation, AlN-based quantum-well (QW) HEMTs offer a promising alternative platform.[12] This structure involves a GaN QW that hosts a two-dimensional electron gas (2DEG), surrounded by AlN buffer and barrier layers. The ultrawide bandgap and high critical electric field of AlN provide a highly electrically insulating buffer with larger breakdown electric fields[13] and higher thermal conductivity than GaN,[14] facilitating efficient heat spreading during device operation.[15] The large polarization discontinuity between AlN and GaN induces a high density 2DEG, even for very thin AlN top barrier layers. This charge is effectively confined by the QW due to the large conduction band offset at the GaN/AlN heterojunctions, making it desirable for high current amplifiers with ultra-scaled gate lengths. Additionally, QW HEMTs grown on single-crystal AlN substrates can provide higher reliability and lower buffer leakage, thanks to their low dislocation densities,[16,17] and the absence of thermal boundary resistance with the substrate.[18]

Despite these potential benefits, 2DEGs in AlN/GaN/AlN QW HEMTs[19–22] have exhibited lower room temperature (RT) electron mobilities compared to Al(Ga)N/GaN HEMTs ($\approx$1900 cm^2/V s). This is likely due to two factors: (1) The high electric field in the GaN QW, which exacerbates scattering[23,24] and (2) Coulomb drag from a 2D hole gas (2DHG) coexisting in the same QW.[25] In this work, we tackle the first factor by investigating the effect of the vertical electric field on the electronic transport of QW HEMTs in a combined experimental and theoretical study of homoepitaxial AlN/GaN/AlN QW HEMTs. The thickness of the well, thus the internal electric field in the

channel, is systematically varied to understand their effect on electron mobility.

A series of binary AlN/GaN/AlN heterostructures schematically depicted in Fig. 1(a) are grown on single-crystal AlN substrates by molecular beam epitaxy (MBE). The thicknesses of the GaN QW (t_w) and AlN barrier (t_b) are both systematically varied across multiple samples with $t_w = \{14, 20, 250\}$ nm and $t_b = \{3, 6\}$ nm. The numerically calculated energy band diagrams shown in Fig. 1(b) show that as the QW thickness increases, the vertical electric field in the GaN QW decreases, resulting in a re-distribution of the electronic wavefunction. The reduction of the electric field shifts the 2DEG centroid away from the interface, decreasing the strength of interface roughness (IR) scattering, therefore enhancing the electron mobility.[26,27] We find that sample C with a thick, relaxed 250-nm-GaN well achieves a high electron density of 3.68×10^{13} cm^{-2} and RT mobility of 823 cm^2/V s, resulting in a record-low RT sheet resistance of 206 Ω/□. Additionally, sample D, featuring a 250-nm-thick GaN well and 2DEG density of 2.53×10^{13} cm^{-2}, demonstrates an RT electron mobility of 1035 cm^2/V s, which shows significant promise in binary QW HEMTs.

The AlN/GaN/AlN double heterostructures were grown on Al-polar single-crystal AlN substrates using a Veeco GEN10 molecular beam epitaxy (MBE) system equipped with Ga and Al standard effusion cells as well as a radio frequency plasma source to supply active nitrogen species. A constant RF plasma power of 200 W with a N_2 gas flow of 0.5 sccm was used, corresponding to a growth rate of 0.24 μm/h. Film growth was monitored *in situ* using KSA Instruments reflection high energy electron diffraction (RHEED) apparatus with a Staib electron gun operating at 14.5 kV and 1.45 A. The single-crystal AlN substrates, with dislocation densities $< 10^4$ cm^2, were provided by Asahi-Kasei Corporation.[28] Prior to epitaxial growth, the substrates underwent a well-defined sequence of preparations, as described in our earlier work.[29] After *ex situ* chemical cleaning in solvents, acids, and a final rinse in de-ionized water, diced AlN substrates were loaded into the MBE system and outgassed at 200 °C for 7 h. Subsequently, the technique of *in situ* Al-assisted surface cleaning was employed, which involves controlled cycles of aluminum adsorption and desorption to effectively remove surface oxide and establish a clean nucleation surface.[29,30]

After Al-assisted surface cleaning, a 500 nm AlN buffer layer was homoepitaxially grown under metal-rich growth conditions, maintaining a constant thermocouple temperature $T_c = 1200$ °C. Excess Al droplets were then thermally desorbed *in situ*. This process was monitored by tracking the recovery of the RHEED intensity during desorption. Subsequently, the substrates were cooled down to $T_c = 850$ °C in preparation for the growth of the GaN channel. The active region was grown continuously, with a deposition sequence of GaN QW, AlN barrier, and GaN cap, all under metal-rich conditions and without any growth interruption. After the epitaxial growth, the substrates were immediately cooled down to RT, and excess Ga droplets were removed *ex situ* using HCl.

To assess the structural quality of our heterostructures, high-resolution x-ray diffraction (HRXRD) is performed for each sample using a Panalytical Empyrean® diffractometer emitting Cu $K_{\alpha 1}$ radiation (1.54 Å). Figure 1(c) shows the diffraction patterns of samples A–D, measured around the (002) symmetric reflection. The theoretical diffraction patterns indicated by the dashed lines in Fig. 1(c) were calculated employing a dynamical diffraction model, and the vertical dashed lines indicate the expected angles for bulk and relaxed AlN and GaN. The AlN peak is observed at the expected relaxed value. As the GaN QW thickness increases, the angle for the GaN diffraction peak is seen to increase and approach its relaxed value, consistent with the decrease in (002) interplanar spacing. The clearly visible interference fringes in thinner QW (samples A and B) suggest sharp heterointerfaces. This allowed for the extraction of each layer's thickness due to the good agreement between the measured and simulated results. However, the disappearance of clear fringes in thick QW (samples C and D) indicated possible degradation in crystal quality due to relaxation process, and, therefore, the thicknesses were estimated based on the growth rate.

To quantify the strain within the GaN channel, reciprocal space maps (RSM) were measured from each sample. Panels (a) through (d)

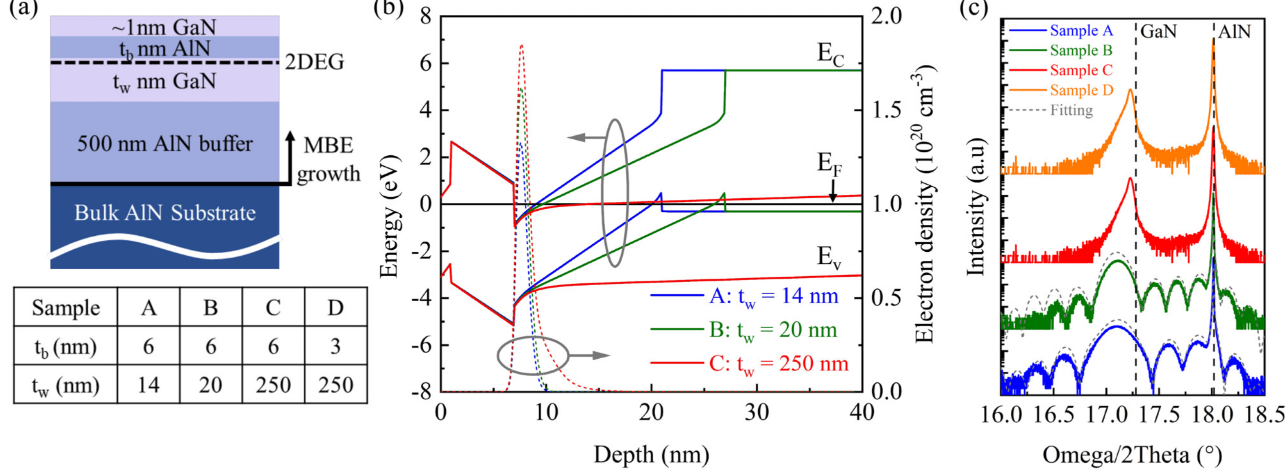

Sample	A	B	C	D
t_b (nm)	6	6	6	3
t_w (nm)	14	20	250	250

FIG. 1. (a) Schematic of the epitaxial heterostructure in this study. (b) The numerically calculated energy band diagrams and electron densities at AlN/GaN interface. (c) Measured (solid lines) and simulated (dashed gray lines) diffraction patterns of samples A–D around the (002) symmetric reflection. The vertical dashed lines indicate the expected angles for bulk, relaxed AlN, and GaN.

10 April 2024 15:51:19

Published under an exclusive license by AIP Publishing

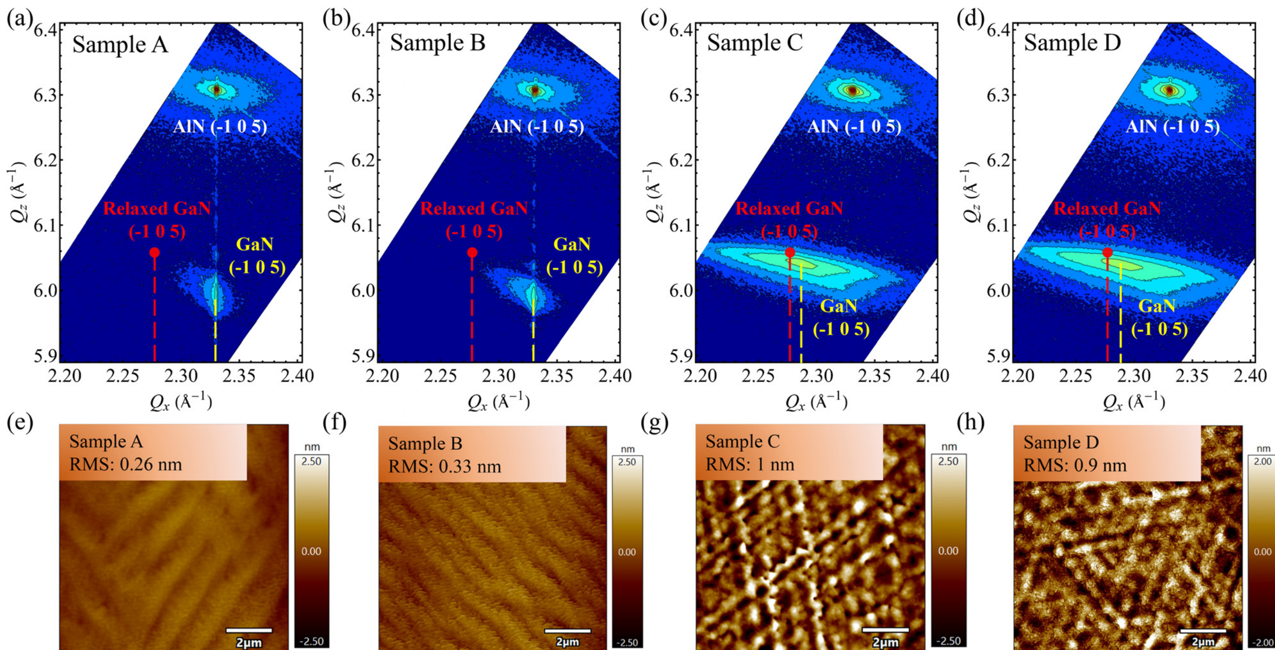

FIG. 2. (a)–(d) RSM around the asymmetric (−105) reflection for samples A–D, respectively. Yellow lines locate the position of strained GaN QW, and red lines indicate the RLPs of relaxed GaN. GaN RLPs shift from a fully strained position toward a fully relaxed position with increasing QW thickness. (e)–(h) 10 × 10 μm^2 AFM of the as-grown samples, showing smooth surface morphologies.

in Fig. 2 display the RSM around the (−105) asymmetric peak of GaN and AlN. The maximum reflection intensity of GaN reciprocal lattice points (RLPs) is observed to shift from a fully strained position toward a fully relaxed position with increasing QW thickness. The broadening of the GaN RLPs indicates defect generation in the QW, which smears out the peaks.[31] The extracted a-lattice constants are as follows: $a^{\text{AlN}} = 3.114$Å for AlN buffer layer, $a^{\text{GaN}} = 3.114$Å for samples A and B, and $a^{\text{GaN}} = 3.17$Å for samples C and D. The in-plane compressive strain of GaN is given by $\epsilon_{xx} = (a^{\text{GaN}} - a_0^{\text{GaN}})/a_0^{\text{GaN}}$. Owing to the smaller lattice constant of the relaxed AlN bulk crystal, the GaN channel in samples A and B exhibits a large compressive strain of −2.3%. However, with an increase in the QW thickness to 250 nm, the compressive strain in the GaN channel decreases to −0.6% (samples C and D).

The effect of the different strain regimes is also seen in the corresponding surface morphologies measured using atomic force microscopy (AFM) with an Asylum Research Cypher ES setup. The AFM scans of samples A and B, shown in Figs. 2(e) and 2(f), reveal atomic steps and smooth surface morphologies with sub-nanometer root mean square (rms) roughness. In contrast, the higher surface roughness of samples C and D with a 250 nm-thick QW stems from the presence of hillocks and cross-hatch morphology of the surface, indicating dislocation formation due to relaxation of the QW [see Figs. 2(g) and 2(h)].

Temperature-dependent electronic transport was characterized by Hall-effect measurements using a Van der Pauw geometry with soldered indium dots as Ohmic contacts. The carrier concentration (n_s), mobility (μ), and sheet resistance (R_s)—at 300 and 10 K—are summarized in Table I and Fig. 3. Panel (a) in Fig. 3 shows the effect of the QW thickness on the 2DEG density, which increases monotonically with t_w. This is due to the lowering of the internal electric field inside the well, thereby reducing the subband energy and enabling a larger electronic population of the well. This trend is in close agreement with the expected density from self-consistent energy band diagram

TABLE I. 2DEG densities (n_s), mobilities (μ), and sheet resistance (R_s) measured via Hall-effect at 300 and 10 K, and calculated internal electric field (F_{avg}) for samples A–D, respectively.

Sample	n_s^{300K} (10^{13} cm^{-2})	μ^{300K} (cm^2/Vs)	R_s^{300K} (Ω/□)	n_s^{10K} (10^{13} cm^{-2})	μ^{10K} (cm^2/Vs)	R_s^{10K} (Ω/□)	F_{avg} (MV/cm)
A	1.99	475	660	1.91	959	341	4.45
B	2.47	618	409	2.40	1290	202	3.90
C	3.68	823	206	3.44	1995	91	2.88
D	2.53	1035	228	2.48	2419	104	2.17

Published under an exclusive license by AIP Publishing

10 April 2024 15:51:19

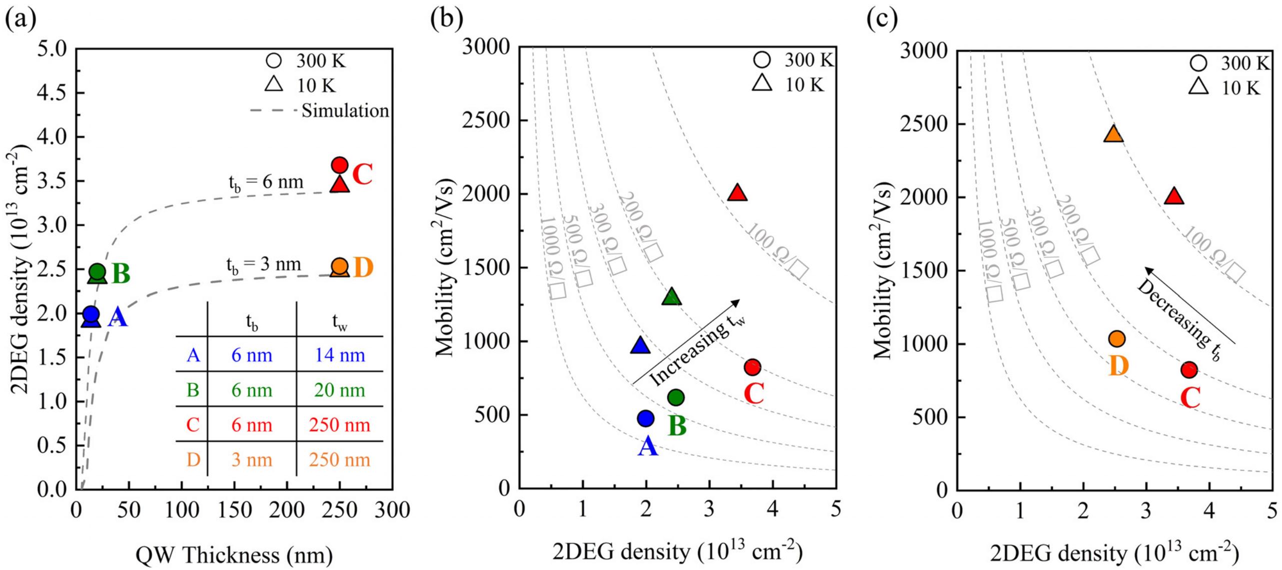

FIG. 3. (a) Measured 2DEG densities for samples A–D at 300 and 10 K, along with the simulated 2DEG density as a function of QW thickness (t_w). (b) Measured mobility vs 2DEG density for samples A–C with different QW thickness (t_w) at 300 and 10 K. (c) Measured mobility vs 2DEG density for samples C–D with different AlN barrier thickness (t_b) at 300 and 10 K.

simulations indicated by the dashed lines in Fig. 3(a). The calculations used a self-consistent Schrödinger–Poisson solver with a surface barrier height of 0.3 eV.[32,33] The measured 2DEG densities remain nearly unchanged down to cryogenic temperatures, confirming their polarization-induced origin. Increasing the QW thickness enhances the 2DEG density, a trend consistently supported by both measured and simulated results. The simulated trend assumes a pseudomorphic growth of GaN on the AlN buffer. However, in cases where the GaN QW relaxes, the 2DEG density is expected to be higher due to tensile strain in the AlN barrier, introducing piezoelectric polarization in the AlN barrier.

Figures 3(b) and 3(c) display the measured mobilities vs 2DEG density for samples A–D at 300 and 10 K. In Fig. 3(b), for samples A–C with a constant AlN barrier thickness ($t_b = 6$ nm), both the 2DEG densities and mobilities increase with the QW thickness. This observed trend is attributed to the reduced internal electric field in the well, leading to a noticeable shift toward the corner of the graph with lower sheet resistance. Notably, sample C, with $t_b/t_w = 6/250$ nm, exhibits a 2DEG density of 3.68×10^{13} cm^{-2} with Hall-mobility of 823 (1995) cm^2/V s at 300 (10) K, resulting in a record-low RT sheet resistance of 206 Ω/□. Enhanced mobility was further achieved by reducing the AlN barrier thickness to 3 nm, as evident when comparing samples C–D in Fig. 3(c). This improvement is due to the further reduced IR and phonon scattering. Sample D, with $t_b/t_w = 3$ nm/250 nm and 2DEG density of 2.53×10^{13} cm^{-2}, demonstrates a Hall-mobility of 1035 (2419) cm^2/V s at 300 (10) K.

It has been a long-standing question whether the 2DHG at the bottom GaN/AlN heterojunction might be influencing the 2DEG mobilities.[34,35] A potential concern arises from the fact that Hall-effect measurements are sampling the parallel conduction of both 2DEG and 2DHG. If parallel conduction originates from two channels with hole and electron densities represented as n_s and p_s, along with corresponding mobilities μ_p and μ_n, then the apparent measured density n_{Hall} and mobility μ_{Hall} at low magnetic field are given by

$$qn_{\text{Hall}} = \frac{(\sigma_n + \sigma_p)^2}{\sigma_p\mu_p - \sigma_n\mu_n}, \quad \text{and} \quad \mu_{\text{Hall}} = \frac{\sigma_p\mu_p + \sigma_n\mu_n}{\sigma_n + \sigma_p},$$

where $\sigma_n = q \times n_s \times \mu_n$ and $\sigma_p = q \times p_s \times \mu_p$ are the conductivities of the two layers and q is the magnitude of the electron charge.[36] The conductivity at low magnetic field is dominated by the higher mobility carriers. Using the above expressions, the 2DEG mobility (μ_n) is extracted from the measured "apparent" Hall mobility (μ_{Hall}). For this analysis, we measured the hole conductivity (σ_p) experimentally in a 2DHG GaN/AlN structure without the AlN top barrier that induced the 2DEG.[37] The schematic of this control sample, grown under identical conditions as the AlN/GaN/AlN heterostructures, and its temperature-dependent Hall-effect measurements are shown in Fig. S1 (supplementary material). Figure S2 presents the measured and extracted 2DEG density and mobility data as a function of temperature for samples A–D. The difference between the extracted and measured 2DEG density is within 10%, and mobility variation is below 5%. Furthermore, conductivity exhibits a noticeable rise as the QW thickness increases, making the error introduced by neglecting the 2DHG in measuring the 2DEG mobility even more negligible. Another concern regarding the presence of 2DHG is the electron–hole scattering in narrow GaN wells, giving rise to Coulomb drag. These carrier-drag effects have been previously measured in modulation-doped GaAs QW, showing a decrease in the momentum relaxation time of electrons at low temperature.[38] In the future, for the AlN/GaN/AlN structures discussed here, we will focus on removing the mobile holes by n-type compensation doping, a strategy that has been previously used in N-polar GaN HEMTs to prevent the formation of the 2DHG.[39,40]

10 April 2024 15:51:19

Published under an exclusive license by AIP Publishing

To identify the scattering mechanisms that limit the channel mobility, we employ temperature-dependent Hall-effect measurements in conjunction with a theoretical transport model, as shown in Fig. 4. The black solid circles are the extracted electron mobilities using the parallel conduction model described earlier. The black lines represent the total calculated mobility according to Matthiessen's rule, including contributions from acoustic phonon (AP), polar optical phonon (POP), and interface roughness (IR) scattering.

Analysis of Fig. 4 reveals that the intrinsic electron mobility at RT is determined predominantly by POP scattering[41] with a weaker contribution by AP scattering.[42] Upon lowering the temperature, the electron mobility increases monotonically due to phonon freeze out, reaching saturation indicating the presence of a temperature-independent IR scattering mechanism. In Figs. 4(a) and 4(b), it is seen that the POP scattering is nearly similar for all samples A–D, and the primary differences at all temperatures arise due to IR scattering.

An explicit expression for the scattering rates due to IR relevant to nitride quantum wells has been previously derived in Refs. 43 and 27. This scattering mechanism exhibits a dependence on the internal electric field ($\mu_{\rm IR} \propto 1/F_{\rm avg}^2$), QW thickness ($\mu_{\rm IR} \propto t_w^6$), roughness ($\mu_{\rm IR} \propto \delta^2$), and screening factor due to the large 2DEG density. The weighted average electric field experienced by the electrons is calculated by $F_{\rm avg} = \frac{\int n(z)\times F(z)\,dz}{\int n(z)\,dz}$, where $n(z)$ and $F(z)$ are the local electron density and electric field, obtained from the self-consistent Schrödinger–Poisson solver, respectively.[44] The statistical properties of the IR are characterized by the correlation length (Λ) and roughness parameter (δ). In this study, Λ is set at 1.25 nm, a value widely used in III-nitride heterojunctions.[45,46] In contrast, δ is treated as a fitting parameter. We found that δ is of the same order of magnitude as the experimentally measured rms roughness, with $\delta \approx 0.3$ nm for samples A and B, and $\delta \approx 0.4$ nm for samples C and D.

Figures 4(a) and 4(b) indicate that the theoretically calculated electron mobilities are in good agreement with the experimentally measured values for all samples. Other scattering mechanisms, such as dislocation scattering and impurity scattering, were also considered but were found to be much weaker than those shown in the same figure. Panel (a) in Fig. 4 compares the temperature dependence of the electron mobility and each individual scattering mechanism across samples with increasing QW thickness. Notably, the strength of the IR scattering decreases monotonically from sample A to sample C as the QW thickness increases. This reduction is primarily attributed to the lowering of the electric field in the channel as the QW thickness increases from 14 to 250 nm. As indicated in Table I, $F_{\rm avg}$ decreases from 4.45 (sample A) to 2.88 MV/cm (sample C) with increasing QW thickness. The diminished electric field shifts the 2DEG centroid away from the interface, mitigating IR scattering influenced by the $1/F_{\rm avg}^2$ dependence. Simultaneously, the thick QW significantly decreases IR scattering due to the t_w^6 dependence. The higher 2DEG density present in thicker QWs provides a better screening of the scattering potential. Despite the higher surface roughness of relaxed QW HEMTs, the reduction in the internal electric field and stronger 2DEG screening outweigh the effects of the roughness. Consequently, these combined factors give rise to the reduction in IR scattering, leading to the observed improvements in mobility and noticeable reduction in sheet resistance to a record-low value $R_s = 206\ \Omega/\square$ at RT in sample C. In contrast, for samples with strained QW layers in samples A and B, the impact of IR scattering outweighs that of phonon scattering, resulting in $\mu_n < 700$ cm^2/V s and $R_s > 400\ \Omega/\square$ (see Table I).

To further improve the electron mobility, we varied the top AlN barrier. The last row of Table I indicates that a thinner AlN barrier of $t_b = 3$ nm reduces the internal electric field in sample D further to approximately 2.17 MV/cm. This results in a shift of the 2DEG centroid away from the interface, lowering the electron density and increasing the mobility. Future changes in heterostructure design to

10 April 2024 15:51:19

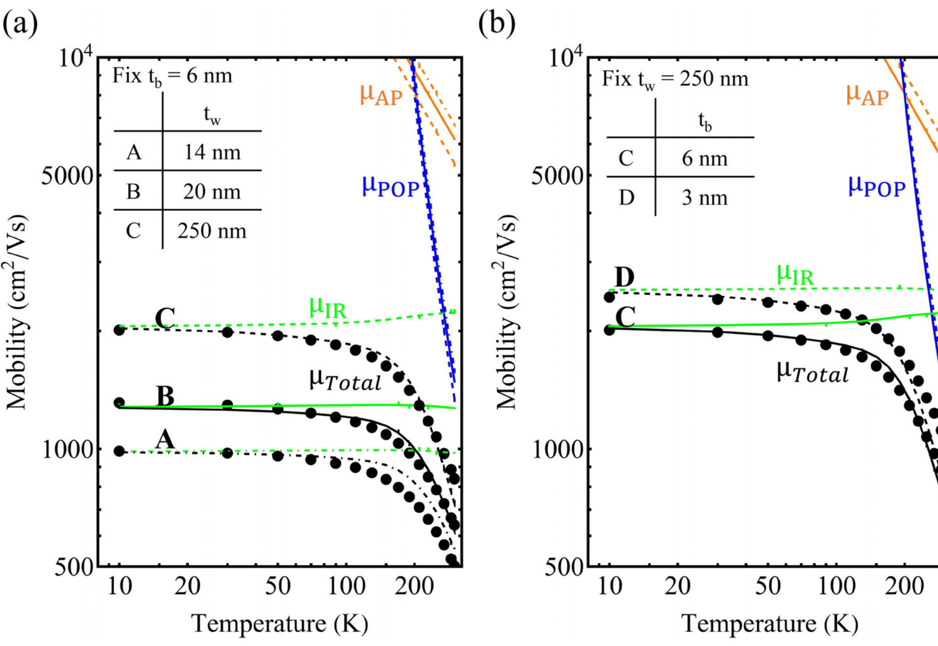

FIG. 4. Temperature dependent Hall-effect measurements with a theoretical transport model. The black solid circles are the extracted electron mobilities using the parallel conduction model. The black lines represent the total calculated mobility according to Matthiessen's rule, including contributions from AP scattering (orange lines), POP scattering (blue lines), and IR scattering (green lines). (a) Comparison between samples A ($t_w = 14$ nm, dot-dashed lines), B ($t_w = 20$ nm, solid lines), and C ($t_w = 250$ nm, dashed lines) with constant t_b of 6 nm. (b) Comparison between samples C ($t_b = 6$ nm, solid lines) and D ($t_b = 3$ nm, dashed lines) with constant t_w of 250 nm.

Published under an exclusive license by AIP Publishing

further reduce the electric field in the well will be useful in elevating electron mobility.

To put these results into perspective, Fig. 5 presents a benchmark comparison of the 2DEG density and RT mobility for the samples in this study, alongside data from previously reported metal-polar Al(Ga)N/GaN/Al(Ga)N[23,47–50] and all binary AlN/GaN/AlN[13,15,19–22,34] heterostructures. The color scale on the right indicates the thickness of the GaN channel. The previous reports include heterostructures grown on different substrates (e.g., SiC, sapphire, and Si) using various growth techniques (metalorganic chemical vapor deposition, metalorganic vapour-phase epitaxy, and MBE). The trend observed is that high electron mobilities are attained for thick and relaxed GaN channels with $n_s \approx 1 \times 10^{13}\ \mathrm{cm}^{-2}$ with the incorporation of alloy AlGaN layers in either the top barrier, or buffer layer, or both (triangles in Fig. 5).[47,49] In the previously reported binary QW HEMTs with AlN top barriers (circles in Fig. 5),[13,15,19–22,34] RT mobility is limited to $800\ \mathrm{cm}^2/\mathrm{V\,s}$. In this work, we demonstrate binary QW HEMTs achieving RT mobility exceeding $1000\ \mathrm{cm}^2/\mathrm{V\,s}$ (sample D). Furthermore, the lowest recorded RT sheet resistance of 206 Ω/□ (sample C) was achieved here among all reported QW HEMTs. However, the price paid in achieving this high mobility and low sheet resistance is the relaxation of the GaN channel, mediated by the generation of dislocations. Previous studies have shown that higher dislocation densities in GaN enhance phonon-dislocation scattering, thereby decreasing its thermal conductivity.[51,52] Therefore, to avoid thermal degradation due to dislocations, methods to reduce the electric field without increasing the GaN channel thickness beyond the critical thickness of relaxation are desired to fully take advantage of the AlN HEMT platform.

In summary, we investigated the electronic transport in AlN/GaN/AlN QW HEMTs by concurrently varying the QW thickness and internal electric field in the well. We demonstrated high-quality growth of binary QW HEMTs on single-crystal AlN substrates, featuring sharp heterointerfaces, smooth surface morphology, and superior electron mobility compared to prior binary QW HEMTs. Through controlled variations in the QW and AlN barrier thickness, we effectively modulated the 2DEG density and mobility by strategically engineering the electric field. Temperature-dependent Hall measurements, combined with theoretical analysis, confirm that IR scattering is the primary mobility-limiting factor in QW HEMTs. By employing a wider QW design to reduce the electric field, we demonstrated RT mobility of $1035\ \mathrm{cm}^2/\mathrm{V\,s}$ with a 2DEG density of $2.53 \times 10^{13}\ \mathrm{cm}^{-2}$ in sample D. Additionally, in sample C, we recorded the lowest RT sheet resistance of 206 Ω/□, outperforming all previously reported QW HEMTs. These breakthroughs open avenues for next-generation high-power RF electronics that take advantage of the high electrical resistivity and thermal conductivity of the AlN platform.

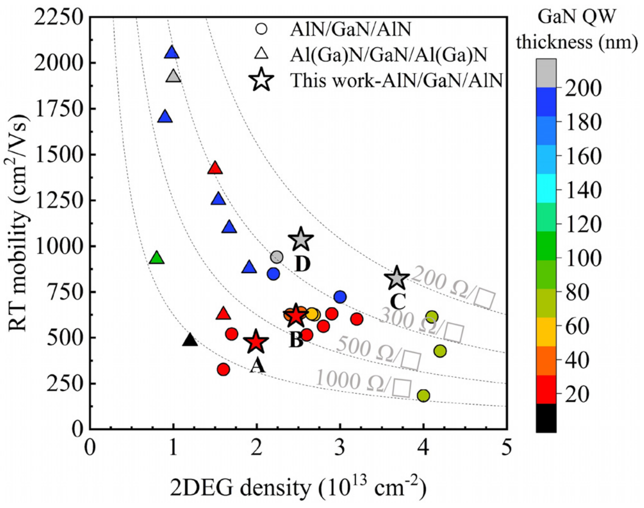

FIG. 5. Benchmark comparison of 2DEG density and RT mobility for samples A–D (stars), alongside the previously reported metal-polar Al(Ga)N/GaN/Al(Ga)N (triangles)[23,47–50] and all binary AlN/GaN/AlN heterostructures (circles).[13,15,19–22,34]

See the supplementary material for the material parameters used for energy band diagram simulation and mobility calculations.

This work was supported by DARPA THREADS program; and ULTRA, an Energy Frontier Research Center funded by the U.S. Department of Energy (DOE), Office of Science, Basic Energy Sciences (BES), under Award No. DE-SC0021230; and SUPREME, one of seven centers in JUMP 2.0, a Semiconductor Research Corporation (SRC) program sponsored by DARPA. This work made use of the Cornell Center for Materials Research (CCMR) Shared Facilities, which are supported through the NSF MRSEC program (No. DMR-1719875), CESI Shared Facilities partly sponsored by NSF No. MRI DMR-1631282, and Kavli Institute at Cornell (KIC).

AUTHOR DECLARATIONS

Conflict of Interest

The authors have no conflicts to disclose.

Author Contributions

Yu-Hsin Chen: Conceptualization (lead); Data curation (lead); Formal analysis (lead); Investigation (lead); Methodology (lead); Validation (lead); Writing – original draft (lead); Writing – review & editing (lead). **Jimy Encomendero:** Conceptualization (supporting); Formal analysis (supporting); Investigation (supporting); Methodology (supporting); Validation (supporting); Writing – review & editing (lead). **Chandrashekhar Savant:** Investigation (supporting); Methodology (supporting); Validation (supporting). **Vladimir Protasenko:** Investigation (supporting); Methodology (supporting); Validation (supporting). **Huili (Grace) Xing:** Conceptualization (lead); Funding acquisition (lead); Investigation (supporting); Methodology (supporting); Project administration (lead); Resources (lead); Supervision (lead); Validation (supporting). **Debdeep Jena:** Conceptualization (lead); Funding acquisition (lead); Investigation (supporting); Methodology (supporting); Project administration (lead); Resources (lead); Supervision (lead); Validation (supporting); Writing – review & editing (lead).

DATA AVAILABILITY

The data that support the findings of this study are available from the corresponding author upon reasonable request.

10 April 2024 15:51:19

Published under an exclusive license by AIP Publishing

REFERENCES

[1]M. A. Khan, J. Kuznia, J. Van Hove, N. Pan, and J. Carter, "Observation of a two-dimensional electron gas in low pressure metalorganic chemical vapor deposited GaN-$Al_xGa_{1-x}N$ heterojunctions," Appl. Phys. Lett. **60**, 3027–3029 (1992).

[2]M. Asif Khan, A. Bhattarai, J. Kuznia, and D. Olson, "High electron mobility transistor based on a GaN-$Al_xGa_{1-x}N$ heterojunction," Appl. Phys. Lett. **63**, 1214–1215 (1993).

[3]O. Ambacher, J. Smart, J. Shealy, N. Weimann, K. Chu, M. Murphy, W. Schaff, L. Eastman, R. Dimitrov, L. Wittmer *et al.*, "Two-dimensional electron gases induced by spontaneous and piezoelectric polarization charges in N- and Ga-face AlGaN/GaN heterostructures," J. Appl. Phys. **85**, 3222–3233 (1999).

[4]U. K. Mishra, L. Shen, T. E. Kazior, and Y.-F. Wu, "GaN-based RF power devices and amplifiers," Proc. IEEE **96**, 287–305 (2008).

[5]U. K. Mishra, P. Parikh, and Y.-F. Wu, "AlGaN/GaN HEMTs—An overview of device operation and applications," Proc. IEEE **90**, 1022–1031 (2002).

[6]Y.-F. Wu, M. Moore, A. Saxler, T. Wisleder, and P. Parikh, "40-W/mm double field-plated GaN HEMTs," in *64th Device Research Conference* (IEEE, 2006), pp. 151–152.

[7]M. Rosker, C. Bozada, H. Dietrich, A. Hung, D. Via, S. Binari, E. Vivierios, E. Cohen, and J. Hodiak, "The DARPA wide band gap semiconductors for RF applications (WBGS-RF) program: Phase II results," in Proceedings of the CS ManTech Conference, 2009.

[8]A. Bar-Cohen, J. D. Albrecht, and J. J. Maurer, "Near-junction thermal management for wide bandgap devices," in *IEEE Compound Semiconductor Integrated Circuit Symposium (CSICS)* (IEEE, 2011).

[9]A. Sarua, H. Ji, K. Hilton, D. Wallis, M. J. Uren, T. Martin, and M. Kuball, "Thermal boundary resistance between GaN and substrate in AlGaN/GaN electronic devices," IEEE Trans. Electron Devices **54**, 3152–3158 (2007).

[10]H. C. Nochetto, N. R. Jankowski, and A. Bar-Cohen, "The impact of GaN/substrate thermal boundary resistance on a HEMT device," in *ASME International Mechanical Engineering Congress and Exposition* (ASME, 2011), Vol. 54969, pp. 241–249.

[11]N. Islam, M. F. P. Mohamed, M. F. A. J. Khan, S. Falina, H. Kawarada, and M. Syamsul, "Reliability, applications and challenges of GaN HEMT technology for modern power devices: A review," Crystals **12**, 1581 (2022).

[12]G. Li, R. Wang, J. Guo, J. Verma, Z. Hu, Y. Yue, F. Faria, Y. Cao, M. Kelly, T. Kosel *et al.*, "Ultrathin body GaN-on-insulator quantum well FETs with regrown ohmic contacts," IEEE Electron Device Lett. **33**, 661–663 (2012).

[13]A. Hickman, R. Chaudhuri, S. J. Bader, K. Nomoto, K. Lee, H. G. Xing, and D. Jena, "High breakdown voltage in RF AlN/GaN/AlN quantum well HEMTs," IEEE Electron Device Lett. **40**, 1293–1296 (2019).

[14]R. Rounds, B. Sarkar, A. Klump, C. Hartmann, T. Nagashima, R. Kirste, A. Franke, M. Bickermann, Y. Kumagai, Z. Sitar *et al.*, "Thermal conductivity of single-crystalline AlN," Appl. Phys. Express **11**, 071001 (2018).

[15]A. Hickman, R. Chaudhuri, L. Li, K. Nomoto, S. J. Bader, J. C. Hwang, H. G. Xing, and D. Jena, "First RF power operation of AlN/GaN/AlN HEMTs with 3 A/mm and 3 W/mm at 10 GHz," IEEE J. Electron Devices Soc. **9**, 121–124 (2021).

[16]X. Hu, J. Deng, N. Pala, R. Gaska, M. Shur, C. Chen, J. Yang, G. Simin, M. A. Khan, J. Rojo *et al.*, "AlGaN/GaN heterostructure field-effect transistors on single-crystal bulk AlN," Appl. Phys. Lett. **82**, 1299–1301 (2003).

[17]E. Kim, Z. Zhang, J. Encomendero, J. Singhal, K. Nomoto, A. Hickman, C. Wang, P. Fay, M. Toita, D. Jena *et al.*, "N-polar GaN/AlGaN/AlN high electron mobility transistors on single-crystal bulk AlN substrates," Appl. Phys. Lett. **122**, 092104 (2023).

[18]G. Alvarez-Escalante, R. Page, R. Hu, H. G. Xing, D. Jena, and Z. Tian, "High thermal conductivity and ultrahigh thermal boundary conductance of homoepitaxial AlN thin films," APL Mater. **10**, 011115 (2022).

[19]S. Rennesson, M. Leroux, M. Al Khalfioui, M. Nemoz, S. Chenot, J. Massies, L. Largeau, E. Dogmus, M. Zegaoui, F. Medjdoub *et al.*, "Ultrathin AlN-based HEMTs grown on silicon substrate by NH_3-MBE," Phys. Status Solidi A **215**, 1700640 (2018).

[20]S. Patwal, M. Agrawal, K. Radhakrishnan, T. L. A. Seah, and N. Dharmarasu, "Enhancement of 2D electron gas mobility in an AlN/GaN/AlN double-heterojunction high-electron-mobility transistor by epilayer stress engineering," Phys. Status Solidi A **217**, 1900818 (2020).

[21]M. Qi, G. Li, S. Ganguly, P. Zhao, X. Yan, J. Verma, B. Song, M. Zhu, K. Nomoto, H. G. Xing *et al.*, "Strained GaN quantum-well FETs on single crystal bulk AlN substrates," Appl. Phys. Lett. **110**, 063501 (2017).

[22]S. Islam, M. Qi, B. Song, K. Nomoto, V. Protasenko, J. Wang, S. Rouvimov, P. Fay, H. G. Xing, and D. Jena, "First demonstration of strained AlN/GaN/AlN quantum well FETs on SiC," in *74th Annual Device Research Conference* (IEEE, 2016).

[23]J. Yaita, K. Fukuda, A. Yamada, T. Iwasaki, S. Nakaharai, and J. Kotani, "Improved channel electron mobility through electric field reduction in GaN quantum-well double-heterostructures," IEEE Electron Device Lett. **42**, 1592–1595 (2021).

[24]Z. Fan, J. Li, M. Nakarmi, J. Lin, and H. Jiang, "AlGaN/GaN/AlN quantum-well field-effect transistors with highly resistive AlN epilayers," Appl. Phys. Lett. **88**, 073513 (2006).

[25]G. Li, B. Song, S. Ganguly, M. Zhu, R. Wang, X. Yan, J. Verma, V. Protasenko, H. Grace Xing, and D. Jena, "Two-dimensional electron gases in strained quantum wells for AlN/GaN/AlN double heterostructure field-effect transistors on AlN," Appl. Phys. Lett. **104**, 193506 (2014).

[26]H. Li, S. Wienecke, B. Romanczyk, E. Ahmadi, M. Guidry, X. Zheng, S. Keller, and U. K. Mishra, "Enhanced mobility in vertically scaled N-polar high-electron-mobility transistors using GaN/InGaN composite channels," Appl. Phys. Lett. **112**, 073501 (2018).

[27]U. Singisetti, M. Hoi Wong, and U. K. Mishra, "Interface roughness scattering in ultra-thin N-polar GaN quantum well channels," Appl. Phys. Lett. **101**, 012101 (2012).

[28]R. T. Bondokov, S. P. Branagan, N. Ishigami, J. Grandusky, T. Nagatomi, K. Tatsuta, T. Miebach, and J. J. Chen, "Two-inch aluminum nitride (AIN) single crystal growth for commercial applications," ECS Trans. **104**, 37 (2021).

[29]K. Lee, Y. Cho, L. J. Schowalter, M. Toita, H. G. Xing, and D. Jena, "Surface control and MBE growth diagram for homoepitaxy on single-crystal AlN substrates," Appl. Phys. Lett. **116**, 262102 (2020).

[30]Y. Cho, C. S. Chang, K. Lee, M. Gong, K. Nomoto, M. Toita, L. J. Schowalter, D. A. Muller, D. Jena, and H. G. Xing, "Molecular beam homoepitaxy on bulk AlN enabled by aluminum-assisted surface cleaning," Appl. Phys. Lett. **116**, 172106 (2020).

[31]M. Moram and M. Vickers, "X-ray diffraction of III-nitrides," Rep. Prog. Phys. **72**, 036502 (2009).

[32]K. Köhler, S. Müller, R. Aidam, P. Waltereit, W. Pletschen, L. Kirste, H. Menner, W. Bronner, A. Leuther, R. Quay *et al.*, "Influence of the surface potential on electrical properties of $Al_xGa_{1-x}N$/GaN heterostructures with different Al-content: Effect of growth method," J. Appl. Phys. **107**, 053711 (2010).

[33]P. Waltereit, S. Müller, K. Bellmann, C. Buchheim, R. Goldhahn, K. Köhler, L. Kirste, M. Baeumler, M. Dammann, W. Bronner *et al.*, "Impact of GaN cap thickness on optical, electrical, and device properties in AlGaN/GaN high electron mobility transistor structures," J. Appl. Phys. **106**, 023535 (2009).

[34]R. Chaudhuri, *Integrated Electronics on Aluminum Nitride: Materials and Devices* (Springer Nature, 2022).

[35]H. Condori Quispe, S. Islam, S. Bader, A. Chanana, K. Lee, R. Chaudhuri, A. Nahata, H. Xing, D. Jena, and B. Sensale-Rodriguez, "Terahertz spectroscopy of an electron-hole bilayer system in AlN/GaN/AlN quantum wells," Appl. Phys. Lett. **111**, 073102 (2017).

[36]M. Kane, N. Apsley, D. Anderson, L. Taylor, and T. Kerr, "Parallel conduction in GaAs/$Al_xGa_{1-x}As$ modulation doped heterojunctions," J. Phys. C **18**, 5629 (1985).

[37]Z. Zhang, J. Encomendero, R. Chaudhuri, Y. Cho, V. Protasenko, K. Nomoto, K. Lee, M. Toita, H. G. Xing, and D. Jena, "Polarization-induced 2D hole gases in pseudomorphic undoped GaN/AlN heterostructures on single-crystal AlN substrates," Appl. Phys. Lett. **119**, 162104 (2021).

[38]R. Höpfel, J. Shah, P. Wolff, and A. Gossard, "Electron-hole scattering in GaAs quantum wells," Phys. Rev. B **37**, 6941 (1988).

[39]M. H. Wong, U. Singisetti, J. Lu, J. S. Speck, and U. K. Mishra, "Anomalous output conductance in N-polar GaN high electron mobility transistors," IEEE Trans. Electron Devices **59**, 2988–2995 (2012).

[40]S. Rajan, A. Chini, M. H. Wong, J. S. Speck, and U. K. Mishra, "N-polar GaN/AlGaN/GaN high electron mobility transistors," J. Appl. Phys. **102**, 044501 (2007).

10 April 2024 15:51:19

Published under an exclusive license by AIP Publishing

[41] B. Gelmont, M. Shur, and M. Stroscio, "Polar optical-phonon scattering in three- and two-dimensional electron gases," J. Appl. Phys. **77**, 657–660 (1995).
[42] J. H. Davies, *The Physics of Low-Dimensional Semiconductors: An Introduction* (Cambridge University Press, 1998).
[43] R. K. Jana and D. Jena, "Stark-effect scattering in rough quantum wells," Appl. Phys. Lett. **99**, 012104 (2011).
[44] Z. Zhang, J. Encomendero, E. Kim, J. Singhal, Y. Cho, K. Nomoto, M. Toita, H. G. Xing, and D. Jena, "High-density polarization-induced 2D electron gases in N-polar pseudomorphic undoped GaN/$Al_{0.85}Ga_{0.15}N$ heterostructures on single-crystal AlN substrates," Appl. Phys. Lett. **121**, 082107 (2022).
[45] Y. Cao and D. Jena, "High-mobility window for two-dimensional electron gases at ultrathin AlN/GaN heterojunctions," Appl. Phys. Lett. **90**, 182112 (2007).
[46] Y. Zhang, I. Smorchkova, C. Elsass, S. Keller, J. P. Ibbetson, S. Denbaars, U. K. Mishra, and J. Singh, "Charge control and mobility in AlGaN/GaN transistors: Experimental and theoretical studies," J. Appl. Phys. **87**, 7981–7987 (2000).
[47] J.-T. Chen, J. Bergsten, J. Lu, E. Janzén, M. Thorsell, L. Hultman, N. Rorsman, and O. Kordina, "A GaN–SiC hybrid material for high-frequency and power electronics," Appl. Phys. Lett. **113**, 041605 (2018).
[48] U. Choi, D. Jung, K. Lee, T. Kwak, T. Jang, Y. Nam, B. So, and O. Nam, "The effect of AlN buffer layer on AlGaN/GaN/AlN double-heterostructure high-electron-mobility transistor," Phys. Status Solidi A **217**, 1900694 (2020).
[49] R. Elwaradi, J. Mehta, T. H. Ngo, M. Nemoz, C. Bougerol, F. Medjdoub, and Y. Cordier, "Effects of GaN channel downscaling in AlGaN–GaN high electron mobility transistor structures grown on AlN bulk substrate," J. Appl. Phys. **133**, 145705 (2023).
[50] J. Encomendero, Cornell University, personal communication (2022).
[51] H. Li, R. Hanus, C. A. Polanco, A. Zeidler, G. Koblmüller, Y. K. Koh, and L. Lindsay, "GaN thermal transport limited by the interplay of dislocations and size effects," Phys. Rev. B **102**, 014313 (2020).
[52] K. Termentzidis, M. Isaiev, A. Salnikova, I. Belabbas, D. Lacroix, and J. Kioseoglou, "Impact of screw and edge dislocations on the thermal conductivity of individual nanowires and bulk GaN: A molecular dynamics study," Phys. Chem. Chem. Phys. **20**, 5159–5172 (2018).

10 April 2024 15:51:19

Published under an exclusive license by AIP Publishing